Journal of Molecular Graphics and Modelling 49 (2014) 118–128

Contents lists available at ScienceDirect

Journal of Molecular Graphics and Modelling

journal homepage: www.elsevier.com/locate/JMGM

Classical force field parameters for two high-affinity ligands of FKBP12

Lilian Olivieri[a,b,c,d], Fabrice Gardebien[a,b,c,d,*]

[a] DSIMB, INSERM, U1134, Paris F-75015, France
[b] Université de la Réunion, UMR_S 1134, Faculté des Sciences et Technologies, 15, avenue René Cassin, BP 7151, 97715 Saint Denis Messag Cedex 09, Réunion
[c] Institut National de la Transfusion Sanguine, F-75015 Paris, France
[d] Laboratory of Excellence GR-Ex

ARTICLE INFO

Article history:
Accepted 18 February 2014
Available online 26 February 2014

Keywords:
CHARMM force field
Parametrization
High-affinity ligand
FKBP12
Molecular mechanics

ABSTRACT

FKBP12 is an important target in the treatment of transplant rejection and is also a promising target for cancer and neurodegenerative diseases. We determined for two ligands of nanomolar affinity the set of parameters in the CHARMM force field. The fitting procedure was based on reproducing the quantum chemistry data (distances, angles, and energies). Since the dynamical behavior of such ligands strongly depends on the dihedral angles, care was taken to derive the corresponding parameters. Moreover, since each of the central core region of these two ligands is similar to other known ligands or drugs of other proteins, part at least of these parameters could also be useful for these other ligands.

1. Introduction

FKBP12 is a 12 kDa enzyme found mainly in the cytosol that catalyzes the peptidylprolyl *cis–trans* isomerization. Exogenous ligands such as rapamycin can bind tightly to FKBP12 with an inhibition constant of 0.3 nM [1]. In mammalian cells, rapamycin binds to FKBP12 and the complex formed then inhibits the kinase protein mTOR [2]. Hyperactive mTOR signaling is linked to tumor growth and its down-regulation by rapamycin or analogues is considered as a promising therapeutic approach for cancer treatment [3]. In T cells, the complex FKBP12-rapamycin forms a ternary complex with mTOR, which negatively affects cell survival and proliferation [4]. The other high-affinity ligand FK506, which has an inhibition constant of 0.6 nM, acts in T cells as a dimerization agent between FKBP12 and another protein, calcineurin, and blocks the T-cell responses by inhibiting lymphokine production (though a different signal transduction pathway is involved in this case) [1,5]. The immunosuppressive properties of rapamycin and FK506 are currently used for the treatment of transplant rejection [6,7]. In neurons, the FK506-bound form of the protein has been associated with neuroprotective properties. FKBP12 has also been found to be harmful in Parkinson and other neurodegenerative diseases and, thus, represents a promising target [8]. In the mosquito *Aedes aegypti*, which is responsible for the infectious viral disease dengue, its protein FKBP12 has been shown to play a role in its life cycle; this protein, which shares 71% identity with the human form, is also considered as an attractive pharmacological target [9].

Finally, another interesting application where the FKBP12 ligands might be useful is the treatment of the HIV infection. The properties of the immune blood cells to express FKBP12 have been employed in a strategy to prolong the lifetime of a HIV-1 protease inhibitor [10]. In this work, the authors have tethered a protease inhibitor to a FKBP12 ligand. The resulting hybrid ligand has a dual binding domain that allows its redistribution into the FKBP-expressing blood cells, the latter acting as an efficient reservoir of the protease inhibitor. As a result, the metabolism of the protease inhibitor by cytochrome P450 is reduced and, in mice, the drug halflife is improved by 20-fold. As suggested by the authors, other drug classes and other pathologies might also be treated by this promising approach.

Hence, much effort is directed toward finding FK506 analogues devoid of the undesirable immunosuppressive activity that is functionally associated with the ligand region responsible for calcineurin inhibition. To this end, molecular docking and molecular dynamics represent foremost computational techniques that both depend upon reliable parameters in the force field definition of the protein ligand. In this paper, we report the parameters of two known FKBP12 ligands, **8** and **308**, for the force field CHARMM. These two non-immunosuppressive ligands **8** and **308**, shown in Fig. 1, are examples of high-affinity ligands of this protein: the former has an inhibition constant of 10 nM; the latter a dissociation constant that has been calculated as 40-fold higher than

* Corresponding author at: Université de la Réunion, UMR_S 1134, Faculté des Sciences et Technologies, 15, avenue René Cassin, BP 7151, 97715 Saint Denis Messag Cedex 09, Réunion. Tel.: +262 262 93 86 49; fax: +262 262 93 82 37.
E-mail address: Fabrice.Gardebien@univ-reunion.fr (F. Gardebien).

http://dx.doi.org/10.1016/j.jmgm.2014.02.003
1093-3263/

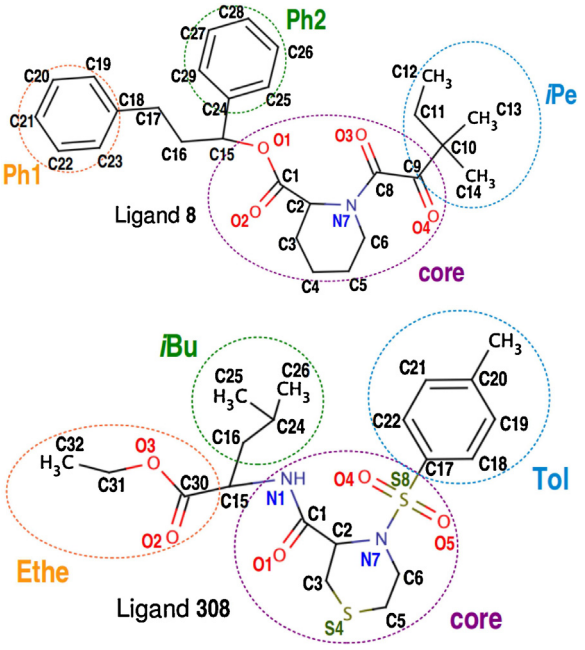

Fig. 1. Two high-affinity ligands, **8** and **308**, of FKBP12 [11,12].

that of rapamycin (the best known ligand of FKBP12), i.e. in the range 8–14 nM [11,12] (the ligands are labeled as in these reference works). Almost all known submicromolar affinity ligands of FKBP12 contain the core structure of the ligand **8** shown in Fig. 1. In numerous analogues of this ligand, its central ring is substituted by a five-membered ring and/or its diketo group substituted by a sulfonamide group, as seen in the ligand **308** in Fig. 1 [13–15]. It should also be stressed that many steric constraints exist in the diketo-pipecolinic acid core region of the ligand **8** due both to the singular geometry of its diketo group and to the ester bond that occupies an axial position of the piperidine ring. Hence, in this work, significant effort was devoted to deriving reliable force field parameters for the cores of these two ligands, especially the dihedral angle parameters found in and around these cores. Since the ligands **8** and **308** represents archetypal high-affinity ligands, these parameters should be valuable for accurate molecular simulation or molecular docking studies of related ligands. Indeed, since either of these cores represents a prerequisite for high-binding properties, adding a substituent in the aromatic rings or changing a peripheral moiety would correspond to a straightforward modification of our parameter set, thus making this set a good start for structurally related ligands.

Force field parameters have been defined to model molecules with great biological interest such as proteins, nucleic acids, lipids, and sugars. The potential energy as calculated with the CHARMM force field is:

$$E = E_{bond} + E_{valence\ \ angle} + E_{Urey\text{-}Bradley} + E_{dihedral\ angle} + E_{improper\ dihedral\ angle} + E_{van\ der\ Waals} + E_{electrostatics} = \sum_{bonds} \frac{1}{2} K_r (r - r_0)^2$$

$$+ \sum_{val.\ ang.} \frac{1}{2} K_\Theta (\Theta - \Theta_0)^2 + \sum_{val.ang.} K_{UB} (UB - UB_0)^2 + \sum_{dih.ang.} K_\Phi (1 + \cos(n\Phi - \delta)) + \sum_{ij} \frac{q_i q_j}{4\pi\epsilon_0 r_{ij}} + \sum_{ij} \epsilon_{ij} \left[\left(\frac{R_{\min,ij}}{r_{ij}} \right)^{12} - 2 \left(\frac{R_{\min,ij}}{r_{ij}} \right)^{6} \right]$$

where r, Θ, UB, and Φ represent the bond length, the valence angle, the Urey-Bradley angle, and the dihedral angle, respectively; ϵ_{ij}, $R_{min,ij}$, r_{ij}, and q_i represent the well depth, the minimum interaction radius, the separation distance, and the charge. Force constants are also used in the first four contributions. More details about these equations are available elsewhere [16,17].

Jorgensen and Pranata indicated that a major difficulty in the simulation of protein–ligand complexes is the lack of parameters for most small organic ligands, including biological or synthetic ligands [18]. To overcome this difficulty, accessible online tools can provide rapidly a set of parameters for a given ligand [19–22]. However, for a better description of the static and dynamic aspects by calculations based on molecular mechanics (MM), the force field developers advise one to define and optimize the parameters for new molecules using a hands-on expertise. As an illustration, the comparison for the two ligands of our dihedral parameters with those derived from CGenFF revealed (i) recurrent shifts in the position of the dihedral minima and (ii) energy barriers that are not consistent with MP2 values. To manually obtain parameters for new molecules that are compatible with the CHARMM force field, we followed the approach that is recommended by the developers of this force field [17].

In the Section 4, the results for the optimization procedure of all the force field parameters are presented for each type of contribution to the potential energy: first, the nonbonded parameters for the atoms of the ligands **8** and **308**; then, the results for the bonded parameters.

2. Materials and methods

The parametrization consists in optimizing the parameters such as to fit the molecular mechanics-derived data to the reference ones (distances, angles or energies) [17]. For the charge fitting, the reference data such as the interaction energies with a water molecule were calculated at the HF/6-31G* level. The energy profiles for the fitting of the valence angles and of the dihedral angles were also obtained at the HF/6-31G* level. However, for the fitting of the dihedral angles, the energies of all the stationary points were obtained by single-point calculations at the MP2/6-31G* level (MP2/6-31G*//HF/6-31G*), since energy barriers at the MP2 level are known to be more reliable. For the dihedral energy calculations, an angle increment of 15° was used for all scans except for torsions around C8—C9 and C9—C10 in ligand **8** for which an increment of 30° was used.

To perform all these ab initio calculations for the two ligands, we used various model molecules that are smaller derivatives of the ligand (Fig. 2). For the charge determination in ligand **8**, the model molecules M81 and M81′ were used; for ligand **308**, the model M3081. For the parameters of the valence angles C3—$\widehat{S4}$—C5 and N7—$\widehat{S8}$—C17, the models M3082 and M3083 were used, respectively. The arrow that appears in all other models in Fig. 2 designates the dihedral angle that was parametrized by using this model.

To allow a comparison with ab initio calculations, all the MM calculations were performed in vacuum without using cut-off distances for the nonbonded interactions. For the geometry optimizations in MM and for the relaxed scans used in dihedral fitting, the ABNR minimization algorithm was used, as recommended by the developers of CHARMM [16].

To optimize the values of the atomic charges, the method we used consists in reproducing the HF interaction energies and distances between a model molecule and a water molecule [23,24].

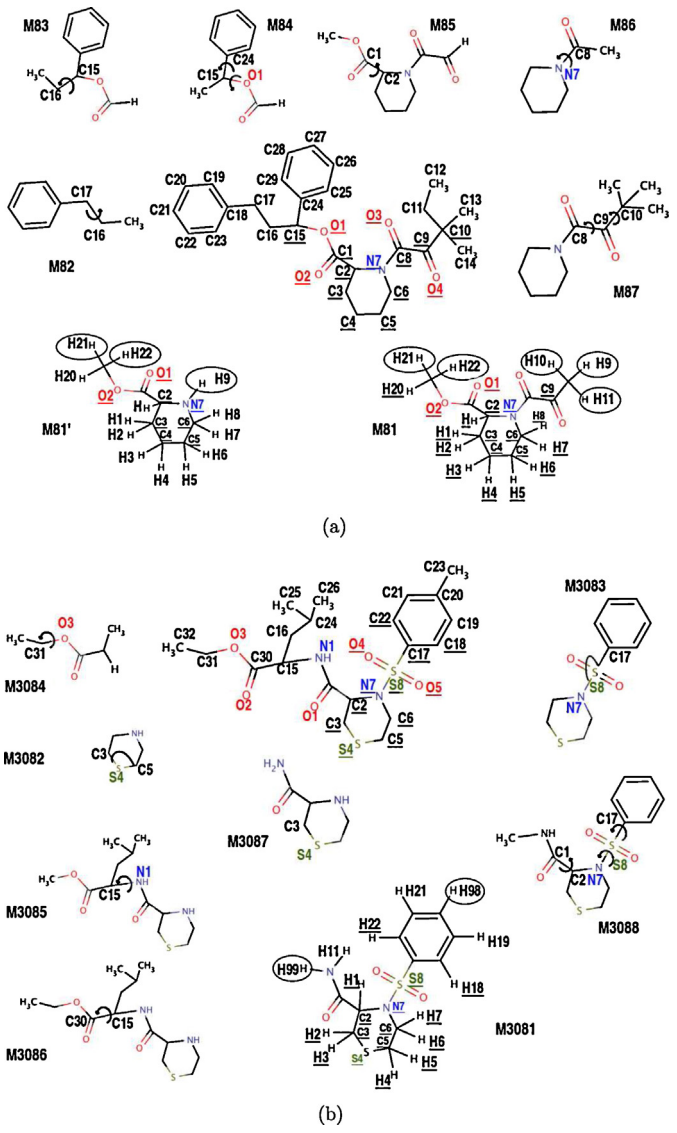

Fig. 2. Model molecules used for the ligand **8** (part a) and **308** (part b). For the model M81 and M3081 used for the charge fitting, the circled hydrogen atom were used in substitution of the original moieties in the respective ligand.

Prior to the ab initio calculations, the model molecule is optimized at the HF/6-31G* level. The HF interaction energies are then derived by orienting a water molecule as hydrogen acceptor or donor and by calculating without geometry relaxation the HF/6-31G* interaction energy between the water and model molecules (rigid scans). This is performed for a range of separation distance. Then, in MM and by using the same model molecule, the HF interaction energy curve is reproduced by fitting the charges. Hence, during these rigid scans, the water molecule can collide with a distant atom of the model molecule. For this reason, the parametrization of a few atoms was not based on the interaction energy profiles (see Section 3). Note that the interaction energy calculated at the MM level depends on the charge of the atom facing the water molecule (O2 or H22 in Fig. 3), but also from the neighboring atoms (such as C1 and C15, respectively, and to a lesser extent to the other atoms bonded to the latter). It is therefore essential to optimize, in a consistent manner, the partial charges of the atoms that are facing the water molecule and those of its neighbors. It is also worth mentioning that, before using the HF interaction energies as reference profiles, the HF energy and distance values must be corrected [17]. First, all the interaction energy values obtained for uncharged atoms

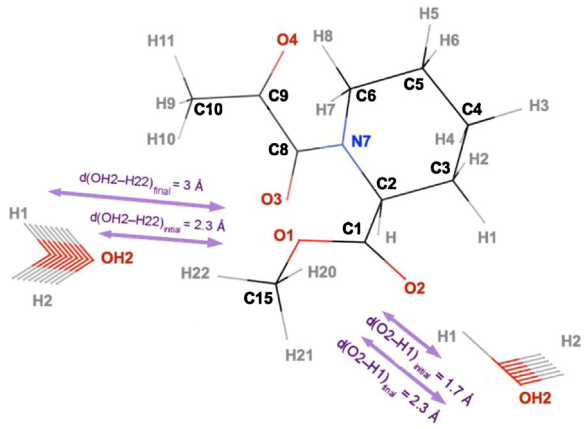

Fig. 3. Model molecule used for the parametrization of the charges of the core atoms in ligand **8**. Two examples of water molecule are superposed: on the left, the rigid scan with step distances of 0.05 Å to obtain the charges on **8**-H22 and -C15; on the right, the same type of scan to determine the charges on **8**-O2 and -C1.

must be multiplied by 1.16. Second, the optimal interaction distance between a water molecule and a polar atom not carrying a net charge must be decreased by 0.20 Å.

The programs Gaussian 03 and GAMESS-US were used for all ab initio calculations. The program CHARMM were used for all MM calculations and for the molecular dynamics simulations in the validation step [25–27]. Whenever indicated in the present work, the parameters of the CHARMM22 version of the CHARMM force field were used.

3. Results

In the text, the atom X of the ligand **8** or **308** is designated as **8**-X or **308**-X.

3.1. Parameters for the van der Waals energy term

The parameters ϵ_i and $R_{min,i}$ were taken from atom types in CHARMM. A direct correspondence exists for all the atoms of the two ligands **8** and **308**, except for the atoms **8**-C9, -C10, -C15, **308**-S8, -N7, and -C17. In Fig. 4(a–d), the correspondence with fragments or molecules that are already defined in CHARMM are described. The new atom types used for both ligands and their correspondence with known atom types in CHARMM are given in Table 7 in the Supplementary data. In the bond sequence N7—C8—C9—C10 of the ligand **8**, the bond N7—C8 can be approximated as an amide bond; however, no equivalent atom can be found in a similar environment for C9 and C10 (the first atom being the β-carbon in a diketone environment and the second being a tertiary carbon adjacent to a carbonyl group). Since the diketone motif is not parametrized, we considered the atom **8**-C9 as an atom type C since this type is used for a carbon atom in double bonds CO that are found in various chemical environments (for **8**-C8 and -C9, the atom type C was redefined as COC in Table 7 in the Supplementary data). For the atom **8**-C15 that is linked to an aromatic carbon, to an aliphatic carbon, and to an oxygen and for which no correspondence was found, the atom type CT1 was considered since this type is also used in various chemical environments (and redefined as COS). For the atom **8**-C10, its contribution to van der Waals interactions with a binding partner such as a protein can be considered negligible as it is surrounded by four carbon atoms; hence, its van der Waals parameters were also taken from those of atom type CT1 (and redefined as CT0).

In ligand **308**, the sulfonamide bond N7—S8—C17 that links two rings has no direct correspondence in CHARMM. Therefore,

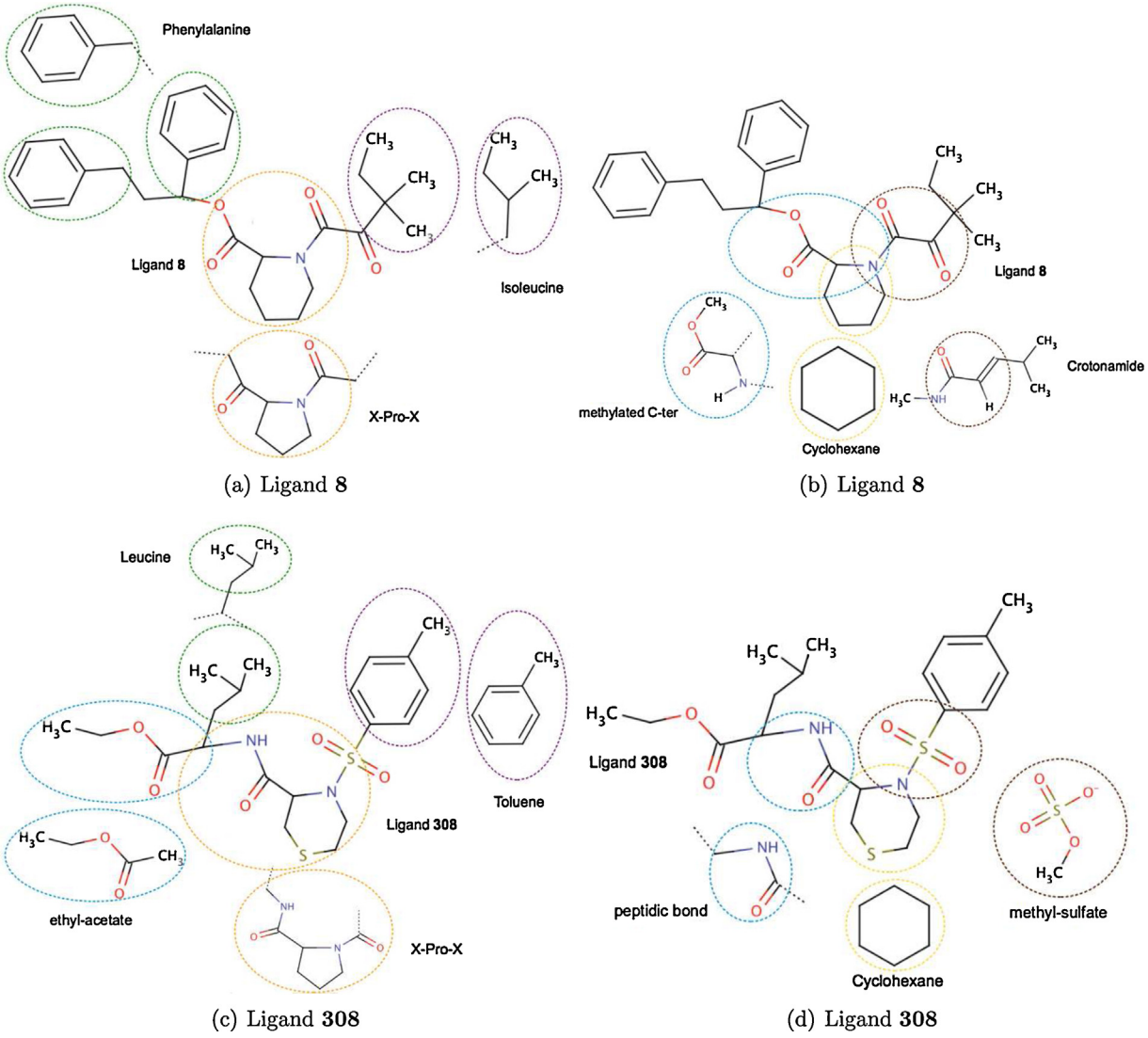

Fig. 4. Correspondences with already parametrized groups of atoms found for a few moieties in ligands **8** ((a) and (b)) and **308** ((c) and (d)).

the assignment of the van der Waals parameters were also based on similarities for these atoms **308**-S8, -N7, and -C17. For the atom **308**-S8, a similarity can be noticed with the environment of a methyl-sulfate that is already parametrized in CHARMM; the parameters of this sulfur atom were then used (Fig. 4(a–d)). Indeed, the comparison of the ϵ_i and $R_{min,i}$ for atom types S, SS, and SL in CHARMM (used for the sulfur atoms found in methionine, thiolates and sulfates such as methyl-sulfate, respectively) indicates only small differences. The respective ϵ_i and $R_{min,i}$ values for the three pairs of these atom types S, SS, and SL differ by, at most, 0.02 kcal/mol for energies and 0.2 Å for distances. Thus, it seems reasonable to use the parameters of the sulfur atom of the methyl sulfate to define the atom **308**-S8. By relying on similar observations for the atoms **308**-N7 and -C17, we also chose to use the van der Waals parameters of the atom N of proline and of the atom C^{γ} of phenylalanine for the atoms **8**/**308**-N7 and **308**-C17, respectively.

3.2. Parameters for the electrostatic energy term

For the charge parametrization, the ligands were cut into four moieties as shown in Fig. 1. Ligands **8** and **308** both consists of regions showing similarities with groups parametrized in CHARMM and of others that need to be parametrized by relying on model molecules. For the peripheral moieties of the ligands that are structurally related with groups of atoms of known parameters, their charges were taken from these groups (see Fig. 4(a–d)). However, the chemical environment was taken into consideration in the charge determination of the Tol moiety in **308** because of possible polarization effect due to the sulfonamide moiety (Tol is the toluene group of **308** encircled in Fig. 1).

In particular, these two ligands have a central portion, the core, that has no correspondence and that is particularly important since it strongly interacts with FKBP. Because no structural match exists for the core of the two ligands, the charges of these atoms were determined. The only exception is the amide bond N1C1O1, seen in the core region of the ligand **308** (Fig. 1), for which the analogy with a peptide bond was used. The model molecules M81 and M3081 shown in Fig. 2 were used for the parametrization of the charges of the hydrogen atoms underlined and of the associated carbon atoms. For the parametrization of the charge of the atom **8**-O1, the structure of M81 model was modified by replacing the group bonded to atom **8**-N7 by a hydrogen atom (Model M81′). In this model, and in contrast to what is observed in M81, there is no steric clashes between the water molecule and the ketone group of **8**-C9 during the scan used to determine the charge. All the charges for the atoms in models M81/M81′ and M3081 were obtained by fitting the HF/6-31G* interaction energy of the atom with a water molecule, as described in Section 2.

Table 1
Distances (d_{opt} in Å) and energies (E_{min} in kcal/mol) for the optimal interactions between a water molecule and the model molecule for ligand **8** (see text and Fig. 2) at the HF and MM levels. For a bond A—B. the atom 1 designates A; the atom 2, B. The charge on the atom N7 is −0.37*e* (see text).

Bond	Charge on atom 1	Charge on atom 2	HF		MM		Difference HF–MM	
			d_{opt}	E_{min}	d_{opt}	E_{min}	Δd_{opt}	ΔE_{min}
C15—H20	0.26	0.01	2.71	−0.97	2.70	−1.21	0.01	0.25
O1	−0.48		1.97	−1.97	2.27	−1.96	−0.30	−0.01
C1—O2	0.84	−0.52	1.89	−4.89	1.80	−4.66	0.09	−0.23
C2—H	0.11	0.05	2.70	0.04	2.60	−0.98	0.10	1.02
C3—H1	−0.18	0.09	2.65	−1.28	2.59	−1.05	0.06	−0.23
C3—H2	−0.18	0.09	2.63	−1.55	2.62	−1.41	0.00	−0.14
C4—H3	−0.18	0.09	2.78	−1.23	2.69	−1.11	0.08	−0.12
C4—H4	−0.18	0.09	2.53	−1.76	2.61	−1.95	−0.08	0.19
C5—H5	−0.20	0.10	2.75	−1.48	2.67	−1.36	0.08	−0.12
C5—H6	−0.20	0.10	2.63	−1.01	2.63	−0.94	0.00	−0.07
C6—H7	−0.09	0.105	2.80	−1.81	2.67	−1.76	0.13	−0.05
C6—H8	−0.09	0.105	2.75	−0.66	2.63	−1.41	0.12	0.75
C8—O3	0.45	−0.46	1.85	−5.19	1.79	−5.15	0.06	−0.04
C9—O4	0.44	−0.40	1.91	−4.39	1.83	−4.44	0.08	0.05
N7	−0.37							

Table 2
Distances (d_{opt} in Å) and energies (E_{min} in kcal/mol) for the optimal interactions between a water molecule and the model molecule for ligand **308** (see text and Fig. 2) at the HF and MM levels. For a bond A—B, the atom 1 designates A; the atom 2, B. The charge on the atom N7 is −0.61*e* (see text).

Bond	Charge on atom 1	Charge on atom 2	HF		MM		Difference HF–MM	
			d_{opt}	E_{min}	d_{opt}	E_{min}	Δd_{opt}	ΔE_{min}
C2—H1	0.09	0.08	2.40	−1.93	2.50	−2.41	−0.10	0.48
C3—H2	−0.18	0.08	2.45	−1.85	2.59	−1.64	−0.14	−0.21
C3—H3	−0.18	0.16	2.45	−1.16	2.56	−1.09	−0.11	−0.07
S4	−0.12		2.70	−1.99	2.42	−1.90	0.28	−0.09
C5—H4	−0.20	0.14	2.40	−1.45	2.58	−1.64	−0.18	0.19
C5—H5	−0.20	0.14	2.55	−2.19	2.57	−2.18	−0.02	−0.01
C6—H6	0.02	0.10	2.70	−1.43	2.58	−2.46	0.12	1.03
C6—H7	0.02	0.08	3.00	−2.77	2.56	−3.14	0.44	0.38
S8—O4	1.70	−0.60	1.90	−4.73	1.78	−4.68	0.12	−0.05
S8—O5	1.70	−0.58	1.88	−4.89	1.78	−4.99	0.10	0.11
C18—H18	−0.03	0.03	2.65	−0.82	2.76	−0.90	−0.11	0.09
C22—H22	−0.03	0.03	2.45	−3.07	2.68	−3.09	−0.23	0.03
N7	−0.61							

We optimized the charges on the hydrogen atoms in the non-aromatic central ring and on the two bonds C18—H18 and C22—H22 in the ligand **308**. For the two latter bonds, this decision was motivated by the polarization effect due to the sulfonamide moiety; for the other hydrogen atoms of the two ligands, the reasons are detailed below and are mainly (i) the through-bond polarization effects due to the amide or sulfonamide moiety (hyperconjugation effect) and (ii) the through-space polarization effects due to numerous oxygen or nitrogen atoms. We decided to optimize simultaneously the charges on both C and H atoms of the CH bonds found in the central rings of the two ligands because the interaction energy between a CH bond and a water molecule strongly depends on the charges on these two atoms. For the same reason, the charges on the double bonds CO and SO were also optimized simultaneously. Hence, the interaction energies with a water molecule and the corresponding distances reported in Tables 1 and 2 for the bonds of type A—B were derived for the optimization of the charges on both atoms.

Table 3
Parameters for the valence angles C3—$\widehat{S4}$—C5 and N7—$\widehat{S8}$—C17 of the ligand **308**. The model molecules that were used in the fitting procedure are also indicated.

Valence angle	Model molecule	K_Θ	Θ_0	K_{UB}	UB_0
C3—$\widehat{S4}$—C5	M3082	58.35	116.96	11.16	2.56
N7—$\widehat{S8}$—C17	M3083	70.00	103.50	–	–

Table 4
Parameters for the eight dihedral angles parametrized in **8**. The model molecule used for the parametrization is also indicated (the corresponding structure is shown in Fig. 2(a)).

Dihedral angle	Model	K_Φ	n	δ
C18—**C17**—**C16**—C15	M82	1.720	3	0.0
		0.300	3	80.0
		0.650	1	0.0
		−0.600	2	180.0
		0.400	2	170.0
C17—**C16**—**C15**—C24	M83	2.050	3	2.1
		0.300	1	−50.0
		0.150	2	275.0
		0.150	1	160.0
C25—**C24**—**C15**—O1	M84	−0.065	2	−89.0
C24—**C15**—**O1**—C1	M84	0.270	3	110.0
		−0.220	1	210.0
		0.220	1	80.0
O1—**C1**—**C2**—N7	M85	1.150	2	60.0
		0.450	1	200.0
		0.100	3	160.0
C2—**N7**—**C8**—O3	M86	12.000	2	−172.2
		0.600	1	200.0
N7—**C8**—**C9**—C10	M87	1.200	1	0.0
		2.600	1	20.0
		−0.800	1	70.0
		0.400	3	120.0
O4—**C9**—**C10**—C11	M87	0.100	3	73.5

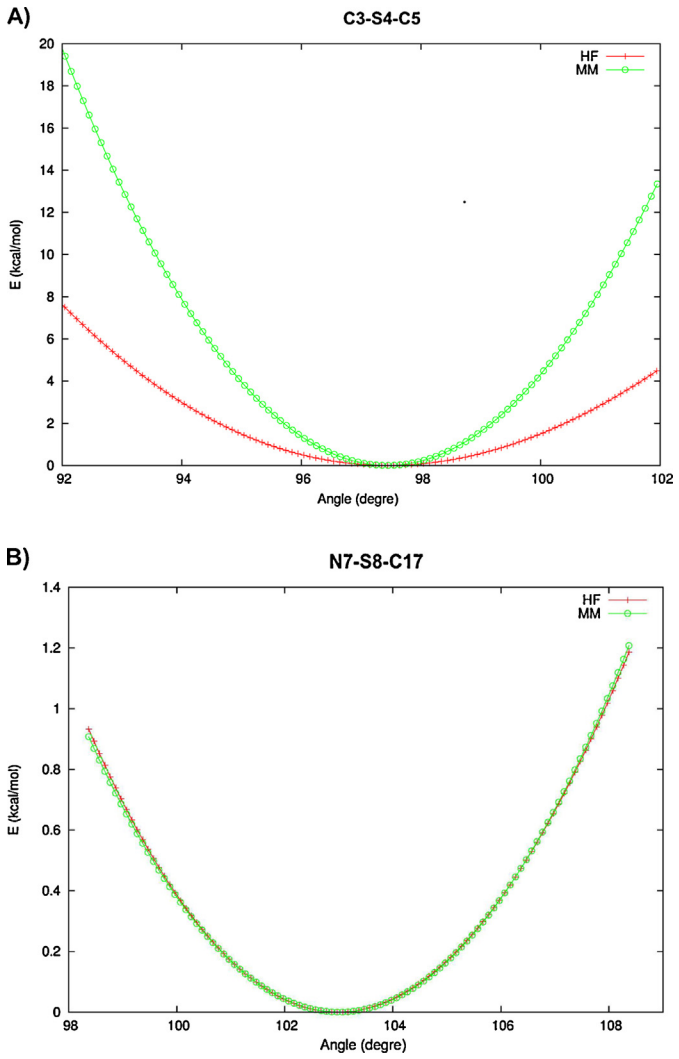

Fig. 5. MM and HF/6-31G* energy profiles for the valence angles C3—$\widehat{S4}$—C5 (A) and N7—$\widehat{S8}$—C17 (B).

3.2.1. Ligand **8**

In the rigid scans performed at the HF and MM levels in order to fit the charges, values for d_{opt} and E_{min} are derived at both energy levels and are shown in Table 1. In this table, the differences between the HF and MM distances (Δd_{opt}) and energies (ΔE_{min}) for optimal interaction does not exceed 0.1 Å and 0.2 kcal/mol in half of the entries, respectively, with small deviations from these values for atoms **8**-H20, -O2, and -H1. A difference Δd_{opt} = 0.3 Å is observed for **8**-O1 that is balanced by a near-zero value of ΔE_{min}. In the crystal structure, the two atoms **8**-H and -H8 (linked to C2 and C6, respectively) are close to the oxygen atoms of the diketone motif: the distance H···O3 and H8···O4 are 2.26 and 2.87 Å, respectively. When the oxygen atom of the water molecule approaches to **8**-H or -H8, the close proximity with the atom **8**-O3 or -O4 leads to HF interaction energies that are larger than from all the other energies reported in Table 1 (below ∼1 kcal/mol). These deviations result from the overlap between the two large electronic densities around the two close oxygen atoms (water oxygen and **8**-O3 or -O4). Thus, a convergence between the MM and HF profiles is difficult to obtain because, on the one hand, of these electronic effects that cannot be captured at the MM level and, on the other hand, of the constraints that we imposed on the hydrogen atom charges. Indeed, the charges on hydrogen atoms were constrained to remain around 0.09*e* (±0.1*e*) so as to be consistent with the charges on hydrogen atoms already parametrized in CHARMM. However, small deviations around this standard hydrogen charge of 0.09*e* were tolerated because of the proximity between the oxygen atoms and the hydrogen atoms of the cycle that cause the polarization of the hydrogen atoms (in addition to O3 and O4, O1 is at 2.49 Å from H7; O2 at 2.64 Å from H1). Hence, for the atom **8**-H, we focused mainly on optimizing all the charges around and then, given the above constraint, a charge was derived on this atom that is associated with a satisfactory value of d_{opt} whereas, despite extensive effort, the value for E_{min} remained far from the optimal HF value. For the atom **8**-H8, the values of the charges on **8**-C6, -H7, and -H8 were optimized simultaneously with the additional constraint for the charges on H7 and H8 to be similar (apart from the above constraint to remain around 0.09*e*). Again, the two values of d_{opt} and one value of E_{min} are in agreement with the HF values whereas the other value of E_{min} associated with C6—H8 is not (for the reason discussed above). Finally, the partial charge of the atom **8**-N7 was adjusted to satisfy the convergence criteria for the interaction between water molecules and its neighboring atoms C2—H, C6—H7/H8, and C8—O3. The water molecule approach toward **8**-N7 on one side of the central ring leads to steric effects with the diketo group (as with **8**-H and H8, see above) and with the axial ester bond for the approach on the other side.

Table 5
Parameters for the seven dihedral angles parametrized in **308**. The model molecule used for the parametrization is also indicated (the corresponding structure is shown in Fig. 2(b)).

Dihedral angle	Model	K_Φ	n	δ
C32—**C31**—**O3**—C30	M3084	0.30	3	0.0
		0.35	2	0.0
O2—**C30**—**C15**—N1	M3086	0.80	3	180.0
		0.80	2	160.0
C16—**C15**—**N1**—C1	M3085	0.90	2	−50.0
		−2.50	1	−90.0
		1.10	1	120.0
N1—**C1**—**C2**—N7	M3088	0.70	3	300.0
		1.75	2	−140.0
		0.50	2	180.0
		0.50	1	0.0
C2—**C3**—**S4**—C5	M3087	3.00	1	80.0
		1.00	1	0.0
C6—**N7**—**S8**—C17	M3088	1.20	2	−30.0
		0.40	4	0.0
		1.50	7	−40.0
		0.50	8	40.0
		0.30	10	210.0
N7—**S8**—**C17**—C18	M3088	−0.80	2	80.0
		0.80	2	0.0
		0.20	6	180.0
		0.45	8	0.0

3.2.2. Ligand ***308***

The three interactions between the water molecule and the bonds C2—H1, H6—C6 and C6—H7 correspond to MM values of E_{min} that differ from HF values by ∼0.4 to ∼1 kcal/mol (Table 2). In this ligand, the polarization effect on the central ring is more important than for the ligand **8** because of all the following short distances between oxygen and ring hydrogen atoms: O4···H1, N1···H6, O5···H7, O5···H4, and C3···H2 are measured in the crystal structure at 2.43, 2.32, 2.81, 2.69, and 2.85 Å, respectively. The sulfur atom S4 has also an influence on the charge distribution around the atoms C3—H1/H2 and C5—H5/H6 of the ring, as indicated by the Mulliken charges (data not shown). Hence, small deviations from the standard charge of 0.09*e* were tolerated during the charge optimization of the hydrogen atoms. In using

the model M3081 to determine the charges for C6—H6 and C6—H7, steric clashes occurred between the water molecule and the amide group C1O1N1 or the Tol moiety, respectively. On the other hand, we observed that the Mulliken charges on all the hydrogen atoms of the non-aromatic cycle are very similar and fall in the range 0.20–0.28*e* for the M3081 geometry optimized at the HF/6-31G* level. Given the above facts, the charges on the atoms C6/H6/H7 resulted (i) from the optimization of those on their neighbors (N7, C5—H4, C5—H5, and S8—O5) and (ii) from the constraint of having similar charges on the hydrogen of the non-aromatic cycle. For the bond C2—H1, the MM interaction energy profile with water is very sensitive to the torsion angle around N7—S8, which is in contrast with the corresponding HF profile. Judging from the N7—S8 torsion profile obtained at the HF level, it should be noted that this torsion angle should have a large amplitude of motion (at least 45° in molecular dynamics simulation at 300 K) around the two minima that are separated by a low energy barrier (see Section 3.5). Therefore, given (i) the conformational dependence of the charges on C2 and H1 and (ii) the high mobility of the sulfonyl group, the charges on these atoms were adjusted by optimizing those on their neighbors (C3—H2, C3—H3, and S8—O4). No interaction energy and distance were specifically calculated for the atom N7 because of the steric clashes with the atoms O4 and O5 for the water molecule approach on one side of the central ring and with the axial amide bond for the approach of the other side. The charge for N7 was derived from the simultaneous optimization of the charges on the neighboring atoms (C3—H2/H3 and S8—O4/O5).

As can be noted from Tables 1 and 2, the values of the charges on C2 and C6 are higher than those on the other carbon atoms of the respective central ring. We correctly reproduced the hyperconjugation effect between the two atoms C2 and C6 and the amide and sulfonamide functions that contributes to the electron density depletion around these two carbons.

3.3. Parameters for covalent bond energy term

3.3.1. Ligand **8**

As indicated in Table 9 in the Supplementary data, for all bonds, a correspondence with bonds that were already parametrized was found; an exception is the C8—C9 bond in the core for which no satisfactory match was found. For this bond, we used the parameters

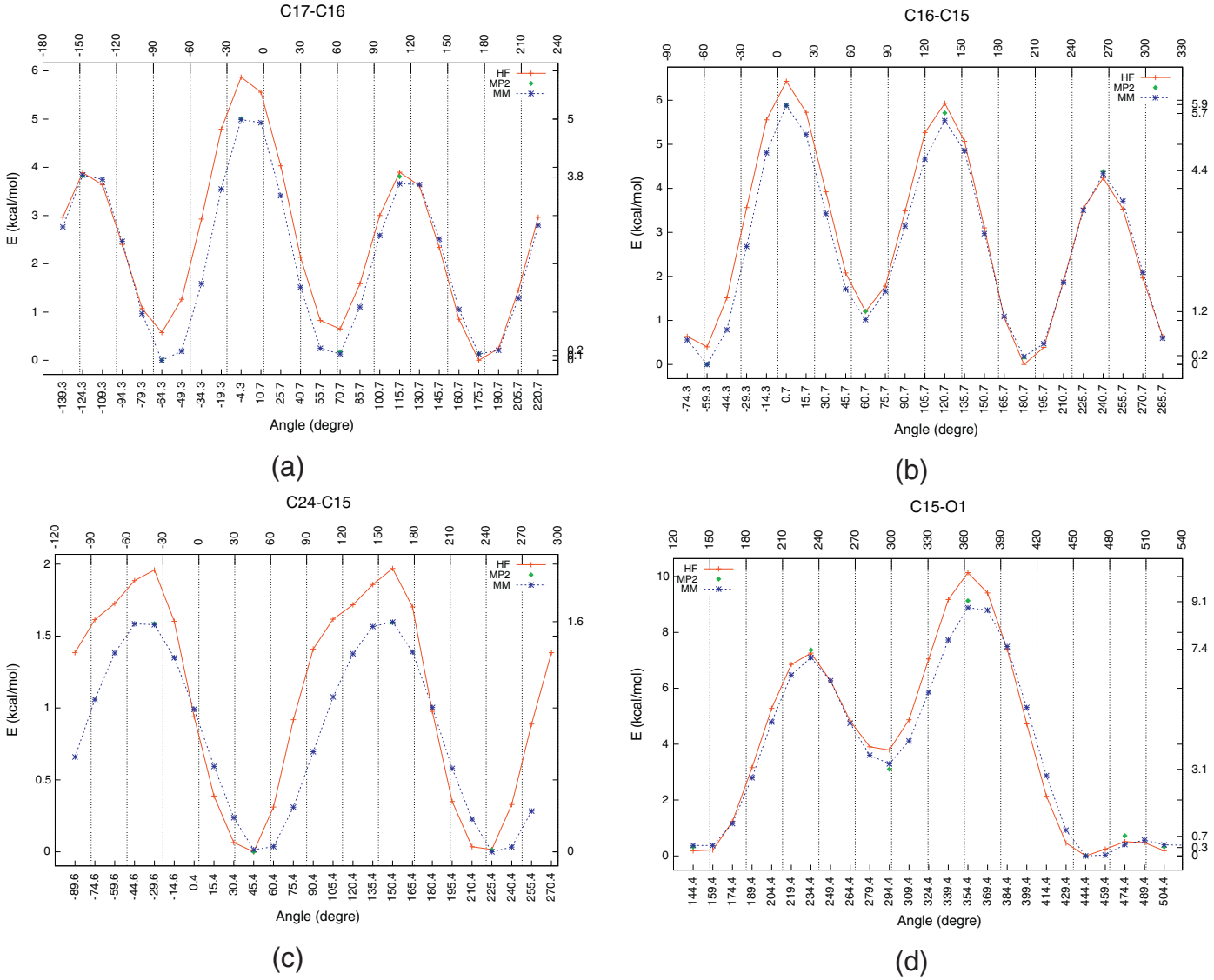

Fig. 6. Energy profiles for the rotation about the bonds C17—C16, C16—C15, C24—C15, C15—O1, C1—C2, N7—C8, C8—C9, and C9—C10 of the ligand **8**. All the MP2 values were obtained at the MP2/6-31G*//HF/6-31G* level. On the *x* axis, the boxed number is the angle value measured in the crystallographic structures.

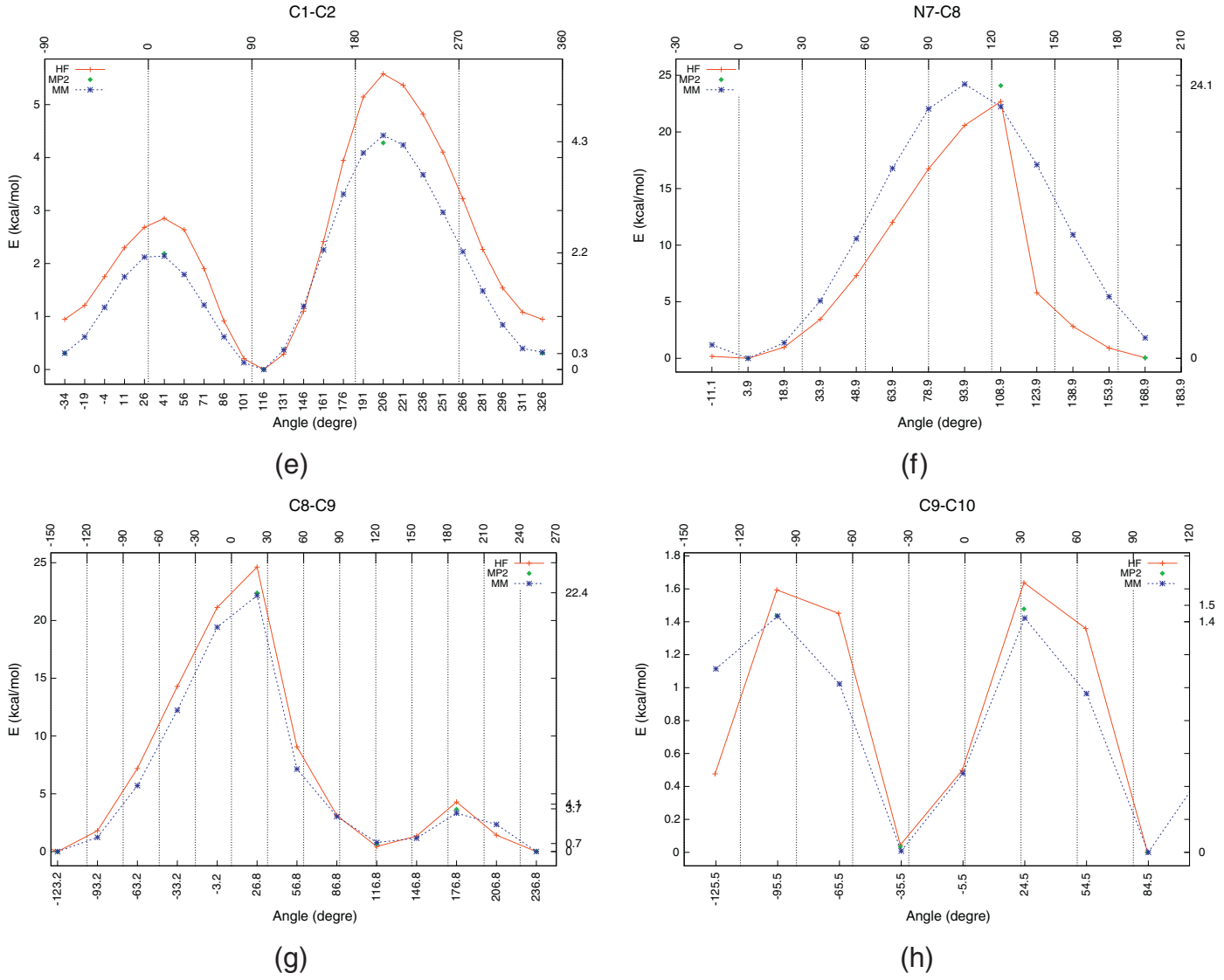

Fig. 6. (*Continued*).

that were obtained from the version CHARMm22 of the force field in the CHARMm module of InsightII [28] (data from the Ligand Protein Database [29]). Though all the parameters of the CHARMm22 force field may not be compatible with those of CHARMM22 (such as charges, van der Waals parameters or torsional barrier heights), we believe that those for covalent bonds may be transferred from CHARMm22 to CHARMM22. The ultimate validation step in Section 4 supports this assumption since, as seen in Table 12 of the Supplementary data, the bond lengths obtained by ab initio and MM geometry optimizations differ only by 0.005 Å.

3.3.2. Ligand ***308***

All the parameters are shown in Table 9. For the covalent bonds C3/C5—S4, instead of using a correspondence with methionine, the parameter K_r is drawn from the one used for the covalent bonds formed between the carbon atoms in the cyclohexane. The value of this parameter remains close to that of the C^{γ}—S bond in methionine and even closer to that found for C—C bonds of the proline ring (229.63, 198 and 222.5 kcal/mol/Å^2 for C3/C5—S4, C^{γ}—S in methionine, and C^{β}—C^{γ} in proline, respectively). For the bonds N7—S8 and C17—S8, the K_r parameters were derived from the S—O single bond in sulfate.

3.4. Parameters for the valence angle and Urey-Bradley energy terms

Most of the parameters used to define the valence angles were transferred from existing parameters in CHARMM (see Table 10 in the Supplementary data). The absence of similarities found for the valence angles C3—$\widehat{S4}$—C5 and N7—$\widehat{S8}$—C17 of the ligand **308**, on one hand, and the wagging motion that one could expect for the Tol moiety in molecular dynamics simulations, one the other hand, prompted us to calculate new parameters for these angles. The parameters obtained are shown in Table 3. In Fig. 5, one can see that the HF and MM energy profiles are in good agreement.

3.5. Parameters for the dihedral angle energy term

Eight and seven dihedral angles were parametrized in **8** and **308**, respectively (as indicated by arrows in Fig. 2). Note that the parameters K_{Φ} were adjusted by fitting the barrier heights in MM to those calculated at the MP2/6-31G*//HF/6-31G* level. More accurate MP2 energies tend to lower the barrier heights in comparison with HF calculations. In Figs. 6 and 7, we can see that all the ab initio profiles along with the associated MP2 minima

and maxima are well reproduced by the MM calculations. The corresponding MM parameters are given in Tables 4 and 5.

For the C3—S4 dihedral energy profiles, the value of this angle in the crystallographic structure is −69.9° and is found in the well around −54.9°. A high energy barrier of 9.1 kcal/mol needs to be overcome to reach a second minimum located at 65.1 or 50.1° calculated at the HF or MM level, respectively. Given this high energy barrier of 9.1 kcal/mol, this second minimum cannot be reached in MD simulations at 300 K. Thus, the corresponding dihedral parameters were optimized to reproduce preferentially the well around −54.9°. For the N7—S8 dihedral energy profiles, a low energy barrier of 0.3 kcal/mol separate the two minima at −67.7° and at −142.7° (with the relative MP2 energies of 1.1 and 0.6 kcal/mol); the transition states nearest from these minima have MP2 values of 7.2 and 6.2 kcal/mol. Thus, two high energy barriers surround these minima, being at 6.1 and 5.6 kcal/mol, respectively. Therefore, we carefully reproduce the MP2 low energy values near the crystallographic dihedral value of −67.7°, including the close minima at −142.7°, and discard the possibility that a transition to another remote minima occurs. This decision was motivated on the basis of a previous study that has shown that an energy threshold of 5 kcal/mol above the global minimum is appropriate for discarding very unlikely ligand binding conformers [30]. Importantly, we reproduce the width of the well that is related to the amplitude of motion. For simulations of the unbound form of the ligand, the MM energy profile for N7—S8, though less precise than around the above-discussed minima, remains qualitatively consistent with that at the HF level.

For the angle around the C17—S8 bond, care was taken to reproduce the low energy barrier found between the global and the local minima (at 247.7 and 292.7°, respectively). The energy barrier associated with this barrier is only 0.3 kcal/mol, indicating an easy conversion between these two minima in molecular dynamics simulations (see Table 6).

4. Validation step

To check the parametrization, we performed MM minimization of the structure of both ligands. The root-mean-square deviations (RMSDs) were then calculated by an alignment with the respective structure optimized at the HF/6-31G* level. The RMSDs for the heavy atoms of the ligands **8** and **308** are 0.63 and 1.28 Å, respectively. RMSDs were also derived by aligning each ligand moiety only. We found that the largest deviations are due to *i*Pe in **8** and to *i*Bu in **308** (RMSDs of 1.2 and 2.2 Å, respectively). The core moiety

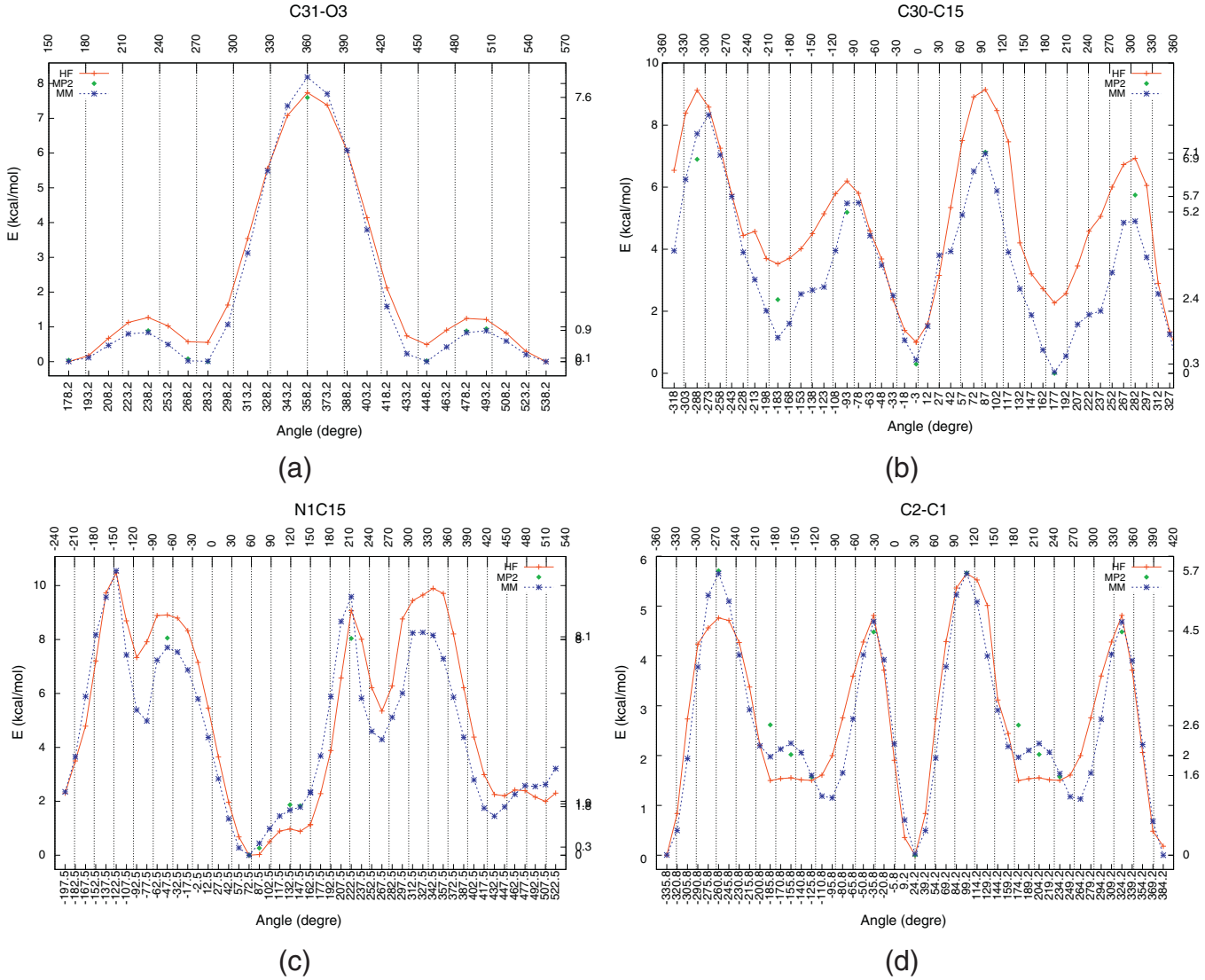

Fig. 7. Energy profiles for the rotation about the bonds C31—O3, C30—C15, C15—N1, C1—C2, C3—S4, N7—S8, and C17—S8 of the ligand **308**. All the MP2 values were obtained at the MP2/6-31G*//HF/6-31G* level. On the *x* axis, the boxed number is the angle value measured in the crystallographic structures.

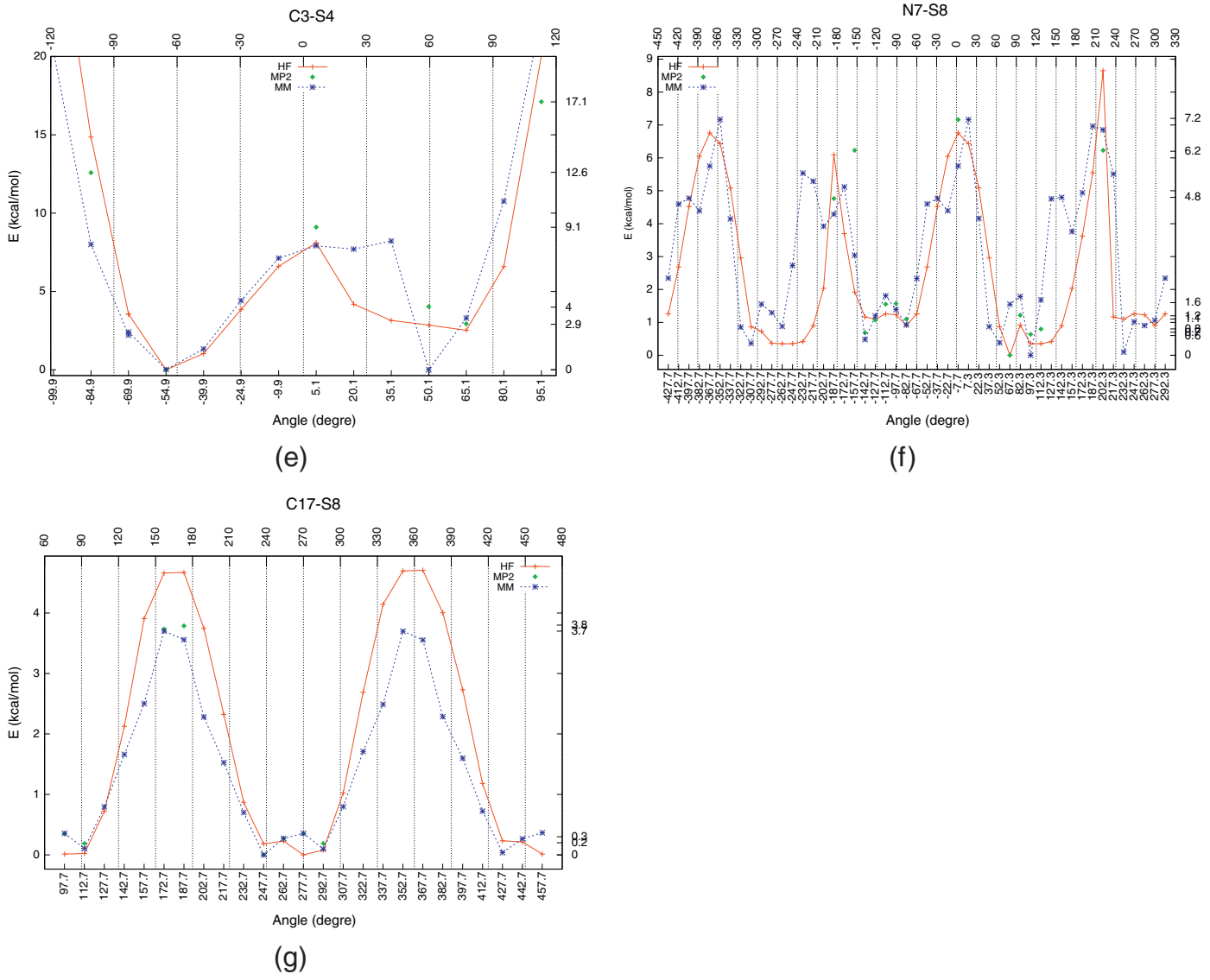

Fig. 7. (*Continued*).

shows the lowest deviations with RMSDs of ∼0.4 in **8** and of ∼0.7 Å in **308**.

In Supplementary data, Tables 12–15 provide the bond distances and valence angles for the two ligands calculated at the HF/6-31G* and MM levels. The reported differences in bond and angles values remain small in both ligand cases, with differences that are found in the intervals [−0.05 ; 0.05 Å] and [−5 ;5°] for all bonds and for all angles, respectively.

Table 6
Parameters for the improper dihedrals labelled A B C D where the central atom is A. Note that the optimal values around atoms C1 and N1 in **308** is not zero, as can be seen in the optimized geometry of this ligand at the HF/6-31G* level.

Improper dihedral	K_{imp}	ϕ_0
C9 O4 C8 C10	120	0.000
C8 O3 N7 C9	120	0.000
C1 O1 O2 C2	120	0.000
N7 C2 C8 C6	4	0.000
C30 C15 O3 O2	100	0
C1 C2 N1 O1	120	−2.4
N1 C1 C15 H11	20	8.3
N7 S8 C2 C6	0	−19.2

In an ultimate validation test, we performed molecular dynamics simulations for the bimolecular system FKBP12-ligand. These last results on the complexes have been published and indicate a good agreement with the respective crystallographic structures in terms of (i) RMSDs for the whole complex and (ii) native intermolecular contacts [31].

5. Conclusion

We have proposed optimized CHARMM force field parameters for two high-affinity ligands of the protein FKBP12. These parameters are useful for modelling techniques such as molecular simulations or molecular docking and should be used instead of parameters that are derived from any technique of automatic assignment. Attention was paid to obtain reliable configurational behavior by carefully fitting all the torsion angles about the bonds that have no satisfactory correspondence in CHARMM. The results of MD simulations performed on the complexes FKBP12-ligand and by using these force field parameters are in good agreement with the crystallographic data available [31].

The sets of parameters are available upon request to the corresponding author.

Acknowledgements

L. Olivieri was the recipient of a doctoral fellowship from the French Ministry of Research. This study was supported by grants from Laboratory of Excellence GR-Ex, reference ANR-11-LABX-0051. The labex GR-Ex is funded by the program 'Investissements d'avenir' of the French National Research Agency, reference ANR-11-IDEX-0005-02. All calculations were performed on the 'Centre de Calcul de l'Université de la Réunion' (CCUR).

Appendix A. Supplementary data

Supplementary data associated with this article can be found, in the online version, at http://dx.doi.org/10.1016/j.jmgm.2014.02.003.

References

[1] M.T. DeCenzo, S.T. Park, B.P. Jarrett, R.A. Aldape, O. Futer, M.A. Murcko, D.J. Livingston, FK506-binding protein mutational analysis: defining the active-site residue contributions to catalysis and the stability of ligand complexes, Protein Eng. 9 (1996) 173–180.
[2] S. Wullschleger, R. Loewith, M.N. Hall, Tor signaling in growth and metabolism, Cell 124 (2006) 471–484.
[3] B.H. Jiang, L.Z. Liu, Role of mTOR in anticancer drug resistance: perspectives for improved drug treatment, Drug Resist. Updat. 11 (2008) 63–76.
[4] B.E. Bierer, P.S. Mattila, R.F. Standaert, L.A. Herzenberg, S.J. Burakoff, G.R. Crabtree, S.L. Schreiber, Two distinct signal transmission pathways in T lymphocytes are inhibited by complexes formed between an immunophilin and either FK506 or rapamycin, Proc. Natl. Acad. Sci. U.S.A. 87 (1990) 9231–9235.
[5] J. Liu, J.D. Farmer, J. Friedman, I. Weissman, S.L. Schreiber, Calcineurin is a common target of cyclophilin-cyclosporin A and FKBP-FK506 complexes, Cell 66 (1991) 807–815.
[6] J.J. Fung, T.E. Starzl, FK506 in solid organ transplantation, Ther. Drug Monit. 17 (1995) 592–595.
[7] G.M. Danovitch, Choice of immunosuppressive drugs and individualization of immunosuppressive therapy for kidney transplant patients, Transplant. Proc. 31 (1999) 2–6.
[8] M. Gerard, A. Deleersnijder, J. Demeulemeester, Z. Debyser, V. Baekelandt, Unraveling the role of peptidyl-prolyl isomerases in neurodegeneration, Mol. Neurobiol. 44 (2011) 13–27.
[9] S. Rajan, K.Q. Saw, Q.T. Nguyen, K. Baek, H.S. Yoon, High-resolution crystal structure of FKBP12 from *Aedes aegypti*, Protein Sci. 21 (2012) 1080–1084.
[10] P.S. Marinec, L. Chen, K.J. Barr, M.W. Mutz, G.R. Crabtree, J.E. Gestwicki, FK506-binding protein (FKBP) partitions a modified HIV protease inhibitor into blood cells and prolongs its lifetime in vivo, Proc. Natl. Acad. Sci. U.S.A. 106 (2009) 1336–1341.
[11] D. Holt, J. Luengo, D. Yamashita, H. Oh, A. Konialian, H. Yen, L. Rozamus, M. Brandt, M. Bossard, M.A. Levy, D.S. Eggleston, J. Liang, L.W. Schultz, T.J. Stout, J. Clardy, Design, synthesis, and kinetic evaluation of high-affinity FKBP ligands and the X-ray crystal structures of their complexes with FKBP12, J. Am. Chem. Soc. 115 (1993) 9925–9938.
[12] F. Sun, P. Li, Y. Ding, L. Wang, M. Bartlam, C. Shu, B. Shen, H. Jiang, S. Li, Z. Rao, Design and structure-based study of new potential FKBP12 inhibitors, Biophys. J. 85 (2003) 3194–3201.
[13] X. Wang, F.A. Etzkorn, Peptidyl-prolyl isomerase inhibitors, Biopolymers 84 (2006) 125–146.
[14] R. Gopalakrishnan, C. Kozany, Y. Wang, S. Schneider, B. Hoogeland, A. Bracher, F. Hausch, Exploration of pipecolate sulfonamides as binders of the FK506-binding proteins 51 and 52, J. Med. Chem. 55 (2012) 4123–4131.
[15] R.E. Babine, S.L. Bender, Molecular recognition of protein–ligand complexes: applications to drug design, Chem. Rev. 97 (1997) 1359–1472.
[16] B.R. Brooks, R. Bruccoleri, B. Olafson, D.J. States, S. Swaminathan, M. Karplus, CHARMM: a program for macromolecular energy, minimization, and dynamics calculations, J. Comput. Chem. 4 (1983) 187–217.
[17] A.D. MacKerell Jr., Atomistic models and force fields, in: O.M. Becker, A.D. MacKerell Jr., B. Roux, M. Watanabe (Eds.), Computational Biochemistry and Biophysics, CRC Press, New York, 2001, pp. 7–38.
[18] J. Pranata, W.L. Jorgensen, Computational studies on FK506: conformational search and molecular dynamics simulation in water, J. Am. Chem. Soc. 113 (1991) 9483–9493.
[19] V. Zoete, M.A. Cuendet, A. Grosdidier, O. Michielin, SwissParam: a fast force field generation tool for small organic molecules, J. Comput. Chem. 32 (2011) 2359–2368.
[20] Topology and parameters for small organic molecules compatible with CHARMM, http://www.swissparam.ch
[21] K. Vanommeslaeghe, E. Hatcher, C. Acharya, S. Kundu, S. Zhong, J. Shim, E. Darian, O. Guvench, P. Lopes, I. Vorobyov, A.D. Mackerell, CHARMM general force field: a force field for drug-like molecules compatible with the CHARMM all-atom additive biological force fields, J. Comput. Chem. 31 (2010) 671–690.
[22] J.D. Yesselman, D.J. Price, J.L. Knight, C.L. Brooks, MATCH: an atom-typing toolset for molecular mechanics force fields, J. Comput. Chem. 33 (2012) 189–202.
[23] W. Reiher, Theoretical studies of hydrogen bonding, Harvard University, 1985 (Ph.D. thesis).
[24] W.L. Jorgensen, Theoretical studies of medium effects on conformational equilibria, J. Phys. Chem. 87 (1983) 5304–5314.
[25] M.J. Frisch, G.W. Trucks, H.B. Schlegel, G.E. Scuseria, M.A. Robb, J.R. Cheeseman, J.A. Montgomery Jr., T. Vreven, K.N. Kudin, J.C. Burant, J.M. Millam, S.S. Iyengar, J. Tomasi, V. Barone, B. Mennucci, M. Cossi, G. Scalmani, N. Rega, G.A. Petersson, H. Nakatsuji, M. Hada, M. Ehara, K. Toyota, R. Fukuda, J. Hasegawa, M. Ishida, T. Nakajima, Y. Honda, O. Kitao, H. Nakai, M. Klene, X. Li, J.E. Knox, H.P. Hratchian, J.B. Cross, V. Bakken, C. Adamo, J. Jaramillo, R. Gomperts, R.E. Stratmann, O. Yazyev, A.J. Austin, R. Cammi, C. Pomelli, J.W. Ochterski, P.Y. Ayala, K. Morokuma, G.A. Voth, P. Salvador, J.J. Dannenberg, V.G. Zakrzewski, S. Dapprich, A.D. Daniels, M.C. Strain, O. Farkas, D.K. Malick, A.D. Rabuck, K. Raghavachari, J.B. Foresman, J.V. Ortiz, Q. Cui, A.G. Baboul, S. Clifford, J. Cioslowski, B.B. Stefanov, G. Liu, A. Liashenko, P. Piskorz, I. Komaromi, R.L. Martin, D.J. Fox, T. Keith, M.A. Al-Laham, C.Y. Peng, A. Nanayakkara, M. Challacombe, P.M.W. Gill, B. Johnson, W. Chen, M.W. Wong, C. Gonzalez, J.A. Pople, Gaussian 03, Gaussian, Inc., Wallingford, CT, 2004.
[26] M.W. Schmidt, K.K. Baldridge, J.A. Boatz, S.T. Elbert, M.S. Gordon, J.H. Jensen, S. Koseki, N. Matsunaga, K.A. Nguyen, S. Su, T.L. Windus, M. Dupuis, J.A. Montgomery, General atomic and molecular electronic structure system, J. Comput. Chem. 14 (1993) 1347–1363.
[27] A.D. MacKerell Jr., D. Bashford, M. Bellott, R. Dunbrack Jr., J. Evanseck, M. Field, S. Fischer, J. Gao, H. Guo, S. Ha, D. Joseph-McCarthy, L. Kuchnir, K. Kuczera, F. Lau, C. Mattos, S. Michnick, T. Ngo, D. Nguyen, B. Prodhom, W. Reiher III, B. Roux, M. Schlenkrich, J. Smith, R. Stote, J. Straub, M. Watanabe, J. Wiorkiewicz-Kuczera, D. Yin, M. Karplus, All-atom empirical potential for molecular modeling and dynamics studies of proteins, J. Phys. Chem. B 102 (1998) 3586–3616.
[28] Accelrys, formerly Molecular Simulation Inc., 9685 Scranton Road, San Diego, CA, 2001.
[29] O. Roche, R. Kiyama, C.L. Brooks III, Ligand–protein database: linking protein–ligand complex structures to binding data, J. Med. Chem. 44 (2001) 3592–3598.
[30] E. Perola, P.S. Charifson, Conformational analysis of drug-like molecules bound to proteins: an extensive study of ligand reorganization upon binding, J. Med. Chem. 47 (2004) 2499–2510.
[31] L. Olivieri, F. Gardebien, Molecular dynamics simulations of a binding intermediate between FKBP12 and a high-affinity ligand, J. Chem. Theory Comput. 7 (2011) 725–741.